

# A Second Higgs Doublet in the Early Universe: Baryogenesis and Gravitational Waves

---

G. C. Dorsch<sup>1</sup>, S. J. Huber<sup>2</sup>, T. Konstandin<sup>1</sup> and J. M. No<sup>2,3</sup>

<sup>1</sup>*DESY, Notkestraße 85, D-22607 Hamburg, Germany*

<sup>2</sup>*Department of Physics and Astronomy, University of Sussex, Brighton BN1 9QH, UK*

<sup>3</sup>*Department of Physics, King's College London, Strand, WC2R 2LS London, UK*

ABSTRACT: We show that simple Two Higgs Doublet models still provide a viable explanation for the matter-antimatter asymmetry of the Universe via electroweak baryogenesis, even after taking into account the recent order-of-magnitude improvement on the electron-EDM experimental bound by the ACME Collaboration. Moreover we show that, in the region of parameter space where baryogenesis is possible, the gravitational wave spectrum generated at the end of the electroweak phase transition is within the sensitivity reach of the future space-based interferometer LISA.

# 1 Introduction

The origin of the baryon asymmetry of the Universe (BAU) remains one of the most important unsolved puzzles in high energy physics and cosmology. Current observations [1, 2] lead to a ratio of the net baryon number per entropy density in the Universe of

$$\eta_{\text{obs}} \equiv \frac{n_B}{s} \simeq 8.7 \times 10^{-11}, \quad (1.1)$$

meaning an excess of roughly one baryon for every one billion matter-antimatter annihilation events taking place in the early Universe. The three necessary ingredients for generating such an asymmetry dynamically [3] are in principle present within the Standard Model (SM): *(i)* baryon number violation due to the chiral anomaly and non-perturbative sphaleron transitions [4–6]; *(ii)* violation of charge (C) and charge-parity (CP) symmetries from the electroweak interactions and quark mixings; *(iii)* displacement from equilibrium coming from the Hubble expansion of the Universe and possibly from the electroweak phase transition (EWPT) [7–9]. A closer analysis indicates, however, that the sphalerons and the CP violating diffusion processes are never simultaneously out of equilibrium with respect to the Hubble expansion [10], so a BAU can only be generated if the process of electroweak symmetry breaking proceeds via a first order phase transition. Kinetic equilibrium would then be broken by the expansion of bubbles of the true vacuum, with a sufficiently large vacuum expectation value (VEV) inside the bubble required in order to avoid washout of the generated asymmetry in the broken phase (see [11] for a recent review on electroweak baryogenesis). As it turns out, this latter condition is *not* satisfied in the SM, since the would-be phase transition is actually a smooth crossover [12, 13]. Furthermore, a second and unrelated problem is the far too small amount of CP violation coming from the CKM matrix, which is suppressed by the Jarlskog invariant [14, 15] as well as by the tiny quark Yukawa couplings, hence leading to a prediction for the BAU which is at best ten orders of magnitude below the observed value [16–18].

The BAU is therefore an observable which asks for an extension of the SM with additional sources of CP violation and extra particles coupling to the Higgs sector. However, the presence of the former has an impact on electric dipole moments (EDMs), which are tightly constrained experimentally. In particular, there has recently been an update on the electron EDM (eEDM) by the ACME collaboration improving the bound by one order of magnitude with respect to the previous experimental limit [19], thus casting doubts on whether certain models would still be viable candidates for successful electroweak baryogenesis, and, if so, which regions of their parameter space would still be allowed. In this work we investigate the current status of baryogenesis in simple Two Higgs Doublet Models (2HDMs)<sup>1</sup>. Previous studies on this problem have already established the *a priori* viability of obtaining the BAU in this framework [21–27], but only one of them takes the ACME eEDM constraint into account [27], albeit with a parameter set that is now excluded

---

<sup>1</sup>A recent work has tackled this issue in the context of 2HDM scenarios with an additional inert singlet. The presence of an extra singlet tends to strengthen the phase transition and therefore decouples the source of a strong EWPT (mainly from the extra singlet) to that of CP violation (which comes from the two doublets), thus alleviating the impact of experimental bounds [20].

by flavor observables. Furthermore, most of these studies assumed a very particular and simplified parameter choice for the study of the EWPT (except for [26]). A more recent analysis of the EWPT in 2HDM scenarios indicates a significantly wider range of parameters allowing for a strong first order transition [28, 29], in particular pointing to regions of the parameter space with a rather exotic phenomenology so far largely unexplored by collider searches [29, 30]. On the other hand, recent analyses on the CP violation front show that the ACME eEDM bound places tight constraints on the CP violating mixing angle among the scalars [31–33]. Whether the amount of allowed CP violation is still sufficient to generate the observed BAU in 2HDMS is a key question we aim to answer in this work.

A first order cosmological phase transition would generate yet another important relic from the early Universe, namely a stochastic gravitational wave (GW) background sourced by the dynamics of scalar field bubbles which generates acoustic waves and possibly turbulence in the plasma at the very end of the transition. For such a source, active at the electroweak scale, the red-shifted spectrum is expected to peak at frequencies  $\mathcal{O}(0.1 - 10 \text{ mHz})$  [34], within the range of detectability of the near-future space-based GW interferometer LISA [35]. The importance of observing such a signal cannot be underestimated: it would not only provide us with a first image of the early Universe beyond the recombination epoch, but would also constitute an alternative, cosmology-based method for probing BSM particle physics which is complementary to collider experiments. The recent measurement of GW from binary black hole mergers by LIGO [36, 37] has already demonstrated our capability to reliably and accurately detect these waves, and has therefore paved the way for using this brand new source of information as a probe of physics from cosmological down to microscopic scales.

It is interesting to note that the baryon asymmetry and the stochastic GW spectrum resulting from the EWPT behave oppositely as a function of the expansion velocity of the scalar field bubbles. Baryogenesis is optimal for relatively slow subsonic bubble walls, allowing enough time for the CP violating diffusion processes to generate an excess of handedness in front of the bubble, later to be converted into a BAU by the sphalerons. On the other hand, a detectable stochastic GW spectrum requires a rather strong phase transition, releasing a large amount of free-energy which can then be converted into bulk motion of the plasma and kinetic energy of the bubbles, thus typically resulting in faster supersonic walls. In particular, when the GW source was modelled as rapidly expanding shells of kinetic energy, after the bubble sphericity has been broken by their collision (the so-called “envelope approximation”), then a sizeable spectrum was usually predicated on ultra-relativistic walls, in which case electroweak baryogenesis is impossible. However, recent developments in the field have significantly improved our understanding of GW generation via acoustic waves [38, 39], which remain active long after bubble collisions end and are therefore a much more efficient source also in the case of deflagrating bubbles<sup>2</sup>. Moreover, it has been noted that the prospective sensitivity of LISA to power-law like spectra can be greatly enhanced by integrating over the frequency of such broadband

---

<sup>2</sup>The impact of turbulence is not yet fully understood, especially the dynamics of its generation from the acoustic waves and the efficiency in converting turbulent movement into GWs. Nevertheless, it is known that turbulence can also remain active long after the phase transition has completed [40].

signals, leading to an improvement of a factor  $\sim \mathcal{O}(10^3)$  with respect to an estimate based only on the raw sensitivity of the apparatus [41]. Using these new developments, we show that the EWPT from 2HDMs could actually lead to *both* an observable BAU and detectable GWs by LISA, as a result of yielding rather strong phase transitions with relatively slow moving bubbles.

## 2 Two-Higgs-Doublet Models

Two Higgs doublet models are among the most minimalistic extensions of the SM, differing from it only by the addition of an extra scalar  $SU(2)_L$  doublet to its field content. In the most general setup the presence of two or more doublets coupling to fermions leads to tree-level flavor changing neutral currents, which require some suppression mechanism for agreement with the highly sensitive experimental data. We impose here a  $\mathbb{Z}_2$  symmetry, forcing each type of fermion to couple to one doublet only [42] (see refs. [43–48] for a few alternatives). Our focus will be on models of Type II, where leptons and down-type quarks couple to  $\Phi_1$  while up-type quarks couple to  $\Phi_2$  [49, 50]. If the  $\mathbb{Z}_2$ -symmetry is exact, however, the scalar sector does not break CP, neither explicitly nor spontaneously [51]. We therefore allow for soft breaking of  $\mathbb{Z}_2$ , in which case the most general renormalizable and gauge-invariant potential for two doublets can be written as

$$\begin{aligned} V_{\text{tree}}(\Phi_1, \Phi_2) = & -\mu_1^2 \Phi_1^\dagger \Phi_1 - \mu_2^2 \Phi_2^\dagger \Phi_2 - \frac{1}{2} \left( \mu^2 \Phi_1^\dagger \Phi_2 + \text{H.c.} \right) + \\ & + \frac{\lambda_1}{2} \left( \Phi_1^\dagger \Phi_1 \right)^2 + \frac{\lambda_2}{2} \left( \Phi_2^\dagger \Phi_2 \right)^2 + \lambda_3 \left( \Phi_1^\dagger \Phi_1 \right) \left( \Phi_2^\dagger \Phi_2 \right) + \\ & + \lambda_4 \left( \Phi_1^\dagger \Phi_2 \right) \left( \Phi_2^\dagger \Phi_1 \right) + \frac{1}{2} \left[ \lambda_5 \left( \Phi_1^\dagger \Phi_2 \right)^2 + \text{H.c.} \right]. \end{aligned} \quad (2.1)$$

Note that  $\mu^2$  and  $\lambda_5$  can be complex, allowing for explicit CP violation in the scalar sector. In this case the VEV of the doublets will also be complex in general, of the form

$$\langle \Phi_1 \rangle = \frac{1}{\sqrt{2}} \begin{pmatrix} 0 \\ v \cos \beta \end{pmatrix}, \quad \langle \Phi_2 \rangle = \frac{1}{\sqrt{2}} \begin{pmatrix} 0 \\ v \sin \beta e^{i\theta} \end{pmatrix}, \quad (2.2)$$

with  $v \approx 246.22$  GeV. However, only two of these three complex phases are a priori independent [52, 53], since a field redefinition can always be used to set one of them to zero. The two field-redefinition-invariant phases can be written as [33]

$$\begin{aligned} \delta_1 &= \text{Arg}[(\mu^2)^2 \lambda_5^*], \\ \delta_2 &= \text{Arg}(v_1 v_2^* \mu^2 \lambda_5^*). \end{aligned} \quad (2.3)$$

Moreover, imposing that  $V_{\text{tree}}$  have a minimum as in eq. (2.2) yields three equations, two of which enable us to trade  $\mu_1^2$  and  $\mu_2^2$  for  $v$  and  $\tan \beta$ , and a third constraining  $\delta_1$  and  $\delta_2$ ,

$$|\mu^2| \sin(\delta_1 - \delta_2) = v^2 \sin \beta \cos \beta |\lambda_5| \sin(\delta_1 - 2\delta_2), \quad (2.4)$$

so that there is ultimately only one free CP violating parameter. Because the CP violating mixing angle between the three neutral scalars must be small due to EDM constraints, it

makes sense to speak of two mostly CP-even mass eigenstates,  $h^0$  and  $H^0$  (with  $m_{H^0} \geq m_{h^0}$ ), and a mostly CP-odd state  $A^0$  (see *e.g.* [32]). A pair of charged scalars  $H^\pm$  then completes the scalar spectrum.

We set  $m_{h^0} = 125$  GeV, identifying the lightest  $h^0$  with the Higgs boson observed at the LHC [54, 55]. A further mixing angle,  $\beta - \alpha$ , regulates how the properties of  $h^0$  relate to those of the SM Higgs  $h_{\text{SM}}$ : in the CP conserving case,  $\beta - \alpha = \pi/2$  corresponds to  $h^0 = h_{\text{SM}}$ , the so-called *alignment limit* [56]. When CP is violated, this equality can never hold exactly since  $h^0$  is not a pure CP-even state. But because the allowed CP violating mixings are small, it is still legitimate to speak of alignment, at least to a good approximation.

## 2.1 Brief Summary of Experimental Constraints

Due to the presence of new scalars mediating loop diagrams, oblique corrections to electroweak precision observables in 2HDMs [57, 58] (see also [59]) can be quite sizeable, particularly affecting the  $\rho \equiv m_W^2/m_Z^2 \cos^2 \theta_W$  parameter. Enforcing  $\rho \approx 1$  leads to an approximate degeneracy between  $H^\pm$  and one of the additional neutral scalars,  $H^0$  or  $A^0$ , this being related to the limit when custodial symmetry is approximately recovered [60, 61]. Moreover, flavor observables whose leading-order contribution in the SM comes from 1-loop diagrams are also highly sensitive to the presence of new scalars. In the  $\mathbb{Z}_2$ -symmetric 2HDM the most important of these are  $\bar{B}_d - B_d$  mixing and  $\bar{B} \rightarrow X_s \gamma$  transitions [62, 63]. For the latter we use the recent NNLO QCD results from [64, 65]. Remarkably, for Type II this yields the stringent bound  $m_{H^\pm} \geq 480$  GeV at 95% C.L.

CP violating phases are tightly constrained by upper bounds on the neutron and electron EDMs. The relevant effective operators are given by [66]

$$\begin{aligned} \mathcal{L} \supset & - \sum_f \frac{d_f}{2} (i \bar{f} \sigma_{\mu\nu} \gamma_5 f F^{\mu\nu}) - \sum_f \frac{\tilde{d}_f}{2} (i g_s \bar{f} \sigma_{\mu\nu} \gamma_5 f T^a G_a^{\mu\nu}) \\ & + \frac{d_W}{6} f_{abc} \epsilon^{\mu\nu\rho\sigma} G_{\mu\lambda}^a G_\nu^\lambda G_{\rho\sigma}^c, \end{aligned} \quad (2.5)$$

with the leading-order contributions to the EDM and chromo-EDM coefficients in 2HDMs,  $d_f$  and  $\tilde{d}_f$ , coming from 2-loop Barr-Zee diagrams, whereas  $d_W$  is generated by the 2-loop Weinberg three-gluon operator [67]. Full expressions can be found in refs. [33, 68]. The chromo-EDM and Weinberg operators affect the neutron EDM via the running down to the nuclear scale  $\Lambda_{\text{QCD}} \sim 1$  GeV, which we perform using the 1-loop RGEs for the Wilson coefficients [69] and 4-loop QCD running of the strong coupling [70].

The results are to be compared to the current 90% C.L. limits for the electron and neutron EDM. For an illustration of the impact of the ACME improved measurement, we also show the constraints from the previous bound coming from experiments done with YbF molecules,

$$|d_e^{\text{ACME}}| < 8.7 \times 10^{-29} \text{ e} \cdot \text{cm}, \quad [19] \quad (2.6)$$

$$|d_e^{\text{YbF}}| < 1.06 \times 10^{-27} \text{ e} \cdot \text{cm}, \quad [71] \quad (2.7)$$

$$|d_n| < 2.9 \times 10^{-26} \text{ e} \cdot \text{cm}. \quad [72] \quad (2.8)$$

### 3 Electroweak Phase Transition and Bubble Wall Velocity

#### 3.1 Electroweak Phase Transition with a Second Higgs Doublet

A strong first order EWPT (as precisely defined in section 3.2) typically requires large couplings to the scalar particles, which in 2HDMs translates to sizable splittings among the scalar masses and/or between these masses and the overall (squared) mass scale of the second doublet,  $M^2 \equiv \text{Re}(\mu^2)/s_{2\beta}$ . Now, in order to avoid the decoupling limit of the second Higgs doublet or instabilities in the scalar potential it is required that<sup>3</sup>  $M \sim v$ . On the other hand, if  $\langle H^0 \rangle \neq 0$  then  $m_{H^0}$  is also required to be light in order to avoid a heavy particle getting a VEV and driving the transition, which would tend to reduce its strength, as occurs in the SM. A relatively heavy  $H^0$  remains possible in the 2HDM alignment limit, where the phase transition is solely driven by  $h^0$ . In this context a tuned, degenerate 2HDM spectrum  $m_{H^0} \simeq m_{A^0} \simeq m_{H^\pm} \gg M \sim v$  can still yield a strong EWPT<sup>4</sup>. This scenario has been studied in [25], and we will not pursue it further here. Still, this highlights that the alignment limit always favours a strong EWPT within the 2HDM, and we will henceforth concentrate on this case for simplicity.

Allowing for sizable splittings among the new scalars significantly enlarges the 2HDM region of parameter space where a strong EWPT is possible [28, 29]. Since electroweak precision observables require  $H^\pm$  to pair with one of the neutral scalars, and  $H^0$  needs to be light if 2HDM alignment is only approximate (for a strong EWPT to be viable), it follows that  $A^0$  is the only scalar which is free to be heavy and induce the required large splittings. Thus, a strong EWPT scenario in 2HDMs generically has a hierarchical spectrum, with  $m_{A^0} - m_{H^0} \gtrsim v$  and  $M \sim m_{H^0} \sim v$  [28, 29].

Since flavour observables constrain  $m_{H^\pm} > 480$  GeV in Type II 2HDM, we choose the pairing  $m_{A^0} = m_{H^\pm}$ , thus arriving at a benchmark scenario with

$$M = m_{H^0} = 200 \text{ GeV}, m_{A^0} = m_{H^\pm} \simeq 480 \text{ GeV} \quad (\text{2HDM Type II in alignment}).$$

We note that for  $1 \leq \tan \beta \leq 5$  the quartic couplings are within the perturbativity bound, with  $\max(\lambda_i) \approx 2\pi$ , and tree-level unitarity is also satisfied [76–78]. We also stress that 2HDM alignment allows for somewhat larger values of  $m_{H^0}$  compatible with a strong EWPT, with a similar hierarchical 2HDM spectrum pattern. This hierarchical pattern can in fact be probed at the LHC through  $A^0 \rightarrow ZH^0$  searches [29], which already constrain our above 2HDM benchmark scenario to  $\tan \beta \gtrsim 1.8$  at 95 % C.L. from LHC Run 1 data [79].

#### 3.2 Phase Transition Strength & Bubble Wall Profile

Since baryogenesis is driven by diffusion processes in front of the bubble wall, we need to compute the temperature  $T_n$  at which bubble nucleation actually starts, i.e. at which the probability of nucleating one bubble within the Hubble horizon  $H^{-1}$  equals unity [9]. This

<sup>3</sup>If  $M \gg v$  and the scalar masses are light, some quartic couplings will be large (in absolute value) and negative, causing the scalar potential to be unbounded from below [73, 74].

<sup>4</sup>For such a spectrum unitarity and perturbativity require  $\tan \beta \simeq 1$ , and any significant departure from this value closes the region of a strong EWPT [75].

can be obtained straightforwardly from the nucleation rate per unit volume [80]

$$\Gamma/\mathcal{V} \simeq T^4 e^{-S_3/T}, \quad (3.1)$$

with  $S_3$  the 3-dimensional action of the associated critical bubble. Once bubbles nucleate, they quickly reach a close to planar steady state, and their profile can then be approximated by an hyperbolic tangent,

$$\begin{pmatrix} h_1(z) \\ h_2(z) \end{pmatrix} = \frac{v_n}{2} \begin{pmatrix} \cos \beta \\ \sin \beta \end{pmatrix} \left[ 1 - \tanh \left( \frac{z}{L_w} \right) \right], \quad (3.2)$$

where  $L_w$  is the wall width and  $v_n = \sqrt{h_1^2(T_n) + h_2^2(T_n)}$  is the VEV at the nucleation temperature. The phase transition strength is given by the ratio  $v_n/T_n$ , and one has a strong first order EWPT when  $v_n/T_n \geq 1$ . A similar expression to (3.2) holds for the CP violating angle  $\theta(z)$  of eq. (2.2), which varies by  $\Delta\theta$  along the bubble wall.

The bubble profile is a saddle point of the action  $S_3$ , and is therefore computed by solving the corresponding equations of motion (EoM) for  $h_1(z)$ ,  $h_2(z)$  and  $\theta(z)$ . While solving this equation is straightforward in a one-dimensional case, for which one can use a simple overshooting-undershooting method, in multi-field cases the problem becomes much more subtle, because one does not know a priori the path along which the shooting is to be performed. Different numerical solutions to this problem have been proposed in the literature [81–84]. Here we take a two-stepped approach inspired by [84]. First, a one-dimensional shooting is performed along the path of the valley connecting both minima of the scalar potential. The resulting profile is then used as a first approximation to the full solution, allowing us to linearize the right hand side of the EoMs by Taylor expanding  $\nabla V$ . The discretized version of the EoMs then becomes a linear system of equations, which can be solved by simple (and computationally cheap) matrix inversion. We have verified that the solution obtained from this method does satisfy the EoMs. In fact, the first step alone provides a very good approximation to the profile parameters.

A top quark penetrating the bubble wall from the symmetric phase acquires a mass

$$m_t(z) = \frac{y_t h_2(z)}{\sqrt{2}} e^{-i\Theta_t(z)}, \quad (3.3)$$

and therefore feels the bubble wall as a potential barrier. In the semiclassical approximation, the complex phase  $\Theta_t$  leads to different dispersion relations for tops and anti-tops, which ultimately induces a non-zero chemical potential for left-handed baryons,  $\mu_{BL}$  [85]. The complex phases  $\Theta_t$  and  $\theta$  are related by [20, 26, 86]

$$\partial_\mu \Theta_t = -\frac{h_1^2(z)}{h_1^2(z) + h_2^2(z)} \partial_\mu \theta. \quad (3.4)$$

Note that due to this relation, which yields  $\Delta\Theta_t = -\Delta\theta/(1 + \tan^2 \beta)$ , there is a suppression for  $\tan \beta \gg 1$ .

The above discussion highlights that the relevant input for the baryon asymmetry computation is the shape of the bubble profile, i.e. the wall thickness  $L_w$ , the phase transition strength  $v_n/T_n$ , and the total change in the top-quark’s CP violating phase,  $\Delta\Theta_t$ . In

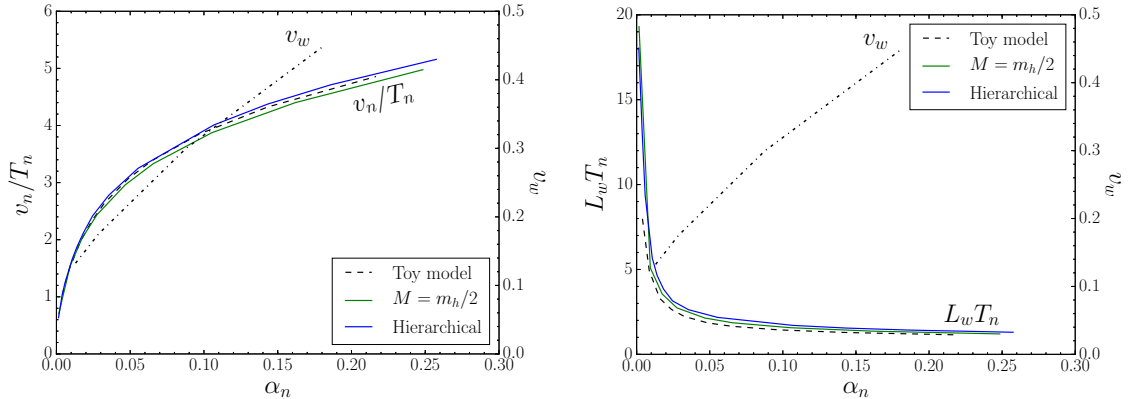


**Figure 1.** Phase transition strength (left) and wall thickness (right) as a function of fractional vacuum energy released in the plasma at nucleation temperature  $T_n$  for the simplified toy model (dashed line), the corresponding 2HDM with  $M = m_h/\sqrt{2}$ ,  $\tan \beta = 1$  and degenerate masses (green solid line) and the hierarchical case considered throughout this work (blue solid line). Also shown are the wall velocities for the toy model (dot-dashed line).

principle there is also a dependence on the wall velocity  $v_w$ , expected to be mild as long as the wall remains subsonic [25].

### 3.3 Bubble Wall Velocity

To estimate  $v_w$  we consider a simplified model with four scalars acquiring masses from their coupling to a SM-like Higgs according to  $m_s = \bar{\lambda}\langle h^0 \rangle/\sqrt{2}$ . This is equivalent to an aligned 2HDM with  $M = m_h/\sqrt{2}$  and  $\tan \beta = 1$ , neglecting the self-interactions of the additional scalars. This latter simplification, together with the fact that the phase transition dynamics in this toy model involves only one scalar field, allows for a more straightforward solution of the EoMs for the scalar field, as is necessary to determine the wall velocity. The friction induced by the fluid is modelled by a single friction parameter,  $\eta$ , following [87]. In a first step, this parameter is determined at the runaway point [88, 89], corresponding to  $\bar{\lambda} = 2.29$ . It is then extrapolated to weaker transitions by applying the scaling  $\eta \sim \exp(-\sqrt{v/T})$  found in [87]. By construction, this procedure correctly reproduces bubble runaway, and leads to a reliable determination of the deflagration/detonation boundary, which is crucial for successful baryogenesis. We show in figure 1 a comparison of the relevant phase transition parameters, namely  $v_n/T_n$ ,  $L_w T_n$  and the fraction of vacuum energy density released in the phase transition in terms of radiation energy in the plasma [89],

$$\alpha_n \equiv \frac{\rho_{\text{vac}}}{\rho_{\text{rad}}}, \quad (3.5)$$

for the toy model, the corresponding 2HDM with  $M = m_h/\sqrt{2}$ , and the hierarchical case considered in the rest of the paper. The parameter  $\alpha_n$ , which will be key for the computation of the GW spectrum from the EWPT, can also be seen as a measure of the phase transition strength: the stronger the transition, the more energy is released into the plasma, leading to greater  $\alpha_n$ . Also shown in figure 1 are the values of the wall velocity for the toy model, which show that bubble walls remain subsonic even for very strong



transitions,  $v_n/T_n \sim 4.0$  and  $\alpha_n \sim 0.15$ . This is the key feature allowing for simultaneous baryogenesis and a detectable stochastic GW signal from the EWPT in the 2HDM. The good agreement between the shape of the bubble profile in the toy model and in the 2HDM, together with the fact that both have the same number of degrees of freedom in the plasma with similar couplings, indicates that these values of  $v_w$  can also be trusted as estimates for the wall velocity in the hierarchical 2HDM considered here.

## 4 Baryogenesis

To compute the baryon asymmetry we use the fluid approximation for the particle distribution functions, with the chemical potential and the fluid velocity as free-parameters. The corresponding linearized Boltzmann equations are then solved for the top, anti-top and bottom quarks, the other particles constituting the background [90]. The source of displacement from thermal equilibrium as well as of CP violation is the bubble profile, i.e. the parameters  $v_n/T_n$ ,  $L_w$  and  $\Delta\Theta_t$ . As discussed in section 3.2, the asymmetric transport of tops and anti-tops along the bubble wall leads to an excess of handedness in front of the wall, represented by a non-vanishing chemical potential,  $\mu_{B_L}$ , for left-handed baryons, to be converted into a baryon asymmetry by the sphalerons (see [91] for more details).

$m_{A^0}$ [GeV]	$T_n$	$v_n/T_n$	$L_w T_n$	$\Delta\Theta_t$	$\alpha_n$	$\beta/H_*$	$v_w$
450	83.665	2.408	3.169	0.0126	0.024	3273.41	0.15
460	76.510	2.770	2.632	0.0083	0.035	2282.42	0.20
480	57.756	3.983	1.714	0.0037	0.104	755.62	0.30
483	53.549	4.349	1.556	0.0031	0.140	557.77	0.35
485	50.297	4.668	1.441	—	0.179	434.80	0.45
487	46.270	5.120	1.309	—	0.250	306.31	$\approx c_s$

**Table 1.** Phase transition parameters relevant for computing the resulting baryon asymmetry (section 4) and the gravitational wave spectrum (section 5), for various pseudoscalar masses  $m_{A^0}$  in the hierarchical scenario presented in section 3. The values are given for fixed  $\tan\beta = 2$ , but only  $\Delta\Theta_t$  is sensitive to  $\tan\beta$  according to 3.4.

The values of the relevant phase transition parameters entering the computation of the baryon asymmetry are shown in Table 1, for varying pseudoscalar masses  $m_{A^0}$  within the hierarchical benchmark discussed in section 3. Notice that for  $m_{A^0} \gtrsim 480$  GeV the phase transition is very strong, leading to very thin bubble walls,  $L_w T_n \sim 1.5$ . This may be problematic for the computation of the baryon asymmetry, since the formalism of top transport is based on a gradient expansion of the Kadanoff-Baym equations [92, 93] with a semi-classical treatment of particles in the plasma, such that their momenta  $p \sim T_n \gg 1/L_w$  [94–96]. To account for possible deviations due to our approaching the extreme bound of validity of these approximations<sup>5</sup>, we conservatively assume that the unforeseen effects lead to an overestimate of the BAU by a factor  $\sim 2$ .

<sup>5</sup>Note that the relevant velocity for baryogenesis is not really  $v_w$ , but the relative velocity between the bubble wall and the plasma in the deflagration front. The latter may be significantly smaller than  $v_w$  [97] in our scenario, yielding a more robust velocity expansion.

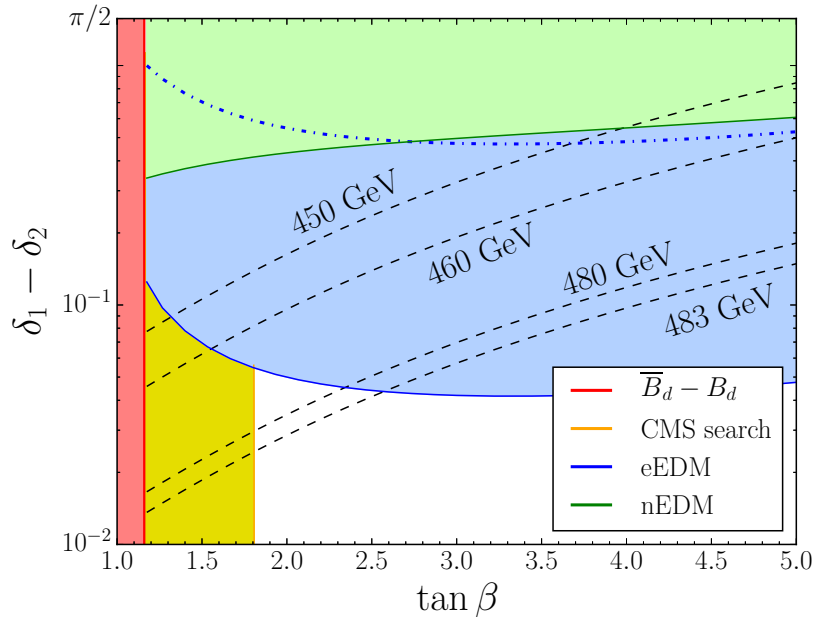


**Figure 2.** EDM constraints for benchmarks described in text. The dash-dotted line corresponds to the eEDM bound before the ACME experiment. The black dashed lines correspond to the minimum CPV phase necessary for successful baryogenesis for  $M = m_{H^0} = 200$  GeV and varying  $m_{A^0} = m_{H^\pm}$ .

Figure 2 shows the minimum value of the complex phase  $\delta_1 - \delta_2$  for which  $\eta_B/\eta_{\text{obs}} = 1$  as a function of  $\tan \beta$ , for  $M = m_{H^0} = 200$  GeV and several values of  $m_{A^0} = m_{H^\pm}$  within the range [450, 490] GeV, corresponding to the hierarchical 2HDM benchmark scenario presented in section 3. As expected, large values of  $\tan \beta$  suppress the generation of the BAU due to eq. (3.4), whose effect has to be compensated by a larger value of  $\delta_1 - \delta_2$  to keep  $\eta_B/\eta_{\text{obs}} = 1$ . The impact of the recent order-of-magnitude improvement on the electron EDM bound from the ACME experiment is highlighted in figure 2 by showing also the exclusion curve (dotted-dashed blue) from the previous eEDM limit. We note that while the neutron-EDM was a competing bound before, the improvement from the ACME experiment now makes the eEDM to provide the dominant constraint by far. Also shown in figure 2 are the excluded regions from  $\overline{B}_d - B_d$  mixing, corresponding to  $\tan \beta \lesssim 1.16$ , and from CMS searches for  $A^0 \rightarrow ZH^0$  with LHC 8 TeV data [79], corresponding (for  $m_{A^0} = 480$  GeV) to  $\tan \beta \lesssim 1.8$ . For  $m_{A^0} \approx 480$  GeV there remains then an allowed window  $1.8 \lesssim \tan \beta \lesssim 2.5$  for which the correct BAU could still be obtained in this scenario. In figure 2 we also present for illustration the results for  $m_{A^0} < 480$  GeV, potentially excluded by the  $\overline{B} \rightarrow X_s \gamma$  flavour bound<sup>6</sup>. The values of the wall thickness in this case are somewhat larger,  $L_w T_n \sim 2 - 3$ , and we can be more confident about the validity of the gradient expansion (nevertheless the curves shown in figure 2 all take into

<sup>6</sup>This is the case for  $m_{A^0} = m_{H^\pm}$ . We however note that a small positive mass splitting  $m_{H^\pm} - m_{A^0}$  is allowed by electroweak precision observables, such as to make the scenario  $m_{A^0} \lesssim 480$  GeV potentially compatible with both constraints.

account the conservative BAU factor  $\sim 2$ , discussed above, for consistency). However, for these values of  $m_{A^0}$  the bounds from CMS searches are even more stringent, excluding  $\tan\beta \lesssim 1.93$ , while the eEDM upper bound on  $\tan\beta$  is also stronger (as a result of a weaker EWPT), altogether closing the baryogenesis window for these masses.

The discussion above emphasizes that, while baryogenesis is still possible within the 2HDM, quite strong phase transitions are required. In fact the usual bound for avoiding sphaleron washout in the broken phase,  $v_n/T_n \gtrsim 1.0$ , turns out being too mild, since EDM constraints alone require significantly stronger transitions if baryogenesis is to be successful.

Before continuing, let us comment on the fact that similar results could have been obtained for an overall mildly heavier spectrum at the cost of tuning. As an example, for  $M = m_{H^0} = 300$  GeV and  $m_{A^0} = m_{H^\pm} \approx 555$  GeV one obtains  $v_n/T_n = 4.513$ ,  $L_w T_n = 1.625$ ,  $\alpha_n = 0.159$  and  $\beta/H_* = 662.85$ , values all similar to those of our previously considered benchmark with  $M = m_{H^0} = 200$  GeV and  $m_{A^0} = m_{H^\pm} \approx 483$  GeV. While the eEDM constraints are hardly affected by this amount of uplifting of the scalar spectrum, bounds from CMS  $A^0 \rightarrow ZH^0$  searches get significantly weakened, being currently insensitive to such heavier spectrum. Note, however, that an increase in  $M = m_{H^0}$  tends to weaken the phase transition, and has to be compensated by larger couplings, thus leading to larger values of  $\beta/H_*$ . As discussed in the next section, even stronger transitions would then be required in order to bring this parameter down to the point where the GW spectrum would be observable at LISA, which in turn would lead to faster walls, thus harming baryogenesis.

Finally, we stress that in the 2HDM of Type II considered here the Barr-Zee diagrams mediated by top and  $W^\pm$  loops interfere destructively, with an optimal cancellation for  $\tan\beta \sim 1$  [27, 32, 33], leading to milder eEDM constraints in this region as manifestly seen in figure 2. This cancellation does not take place in Type I 2HDM, where the EDM bounds are more severe for low  $\tan\beta$ , precisely where baryogenesis is optimal. This shows that accommodating successful baryogenesis in Type I 2HDMs is more challenging.

## 5 Gravitational Wave Spectrum

While baryogenesis takes place during the period of bubble expansion, gravitational waves start getting sourced at the end of the phase transition, when the bubbles collide and overlap. One such source is the uncolliding expanding envelopes of scalar field bubbles, since the bubbles' spherical symmetry is broken by their partial overlap. For thermal phase transitions, such as the one we are considering here, where the bubble wall has reached a constant velocity long before the bubbles collide, the scalar field contribution is tiny and can be completely ignored. Practically the entire energy released by the transition goes into the plasma, as heat and fluid motion. As numerical simulations show [39], the collision of bubbles produces fluid perturbations mostly in the form of sound waves in the plasma, which act as a long lived, powerful source of gravitational waves, until they are switched off by the Hubble expansion. For sufficiently strong transitions one also expects

that the sound waves turn into a stage of turbulence before a Hubble time [98, 99], with the turbulent fluid also acting as a GW source [40].

The amplitude of the GW spectrum depends crucially on the amount of energy released in the phase transition and available to be converted into GWs, i.e. the  $\alpha$  parameter in eq. (3.5). Another important quantity is the (approximate) inverse duration of the phase transition,  $\beta$ , given in terms of the Hubble rate by

$$\frac{\beta}{H_*} = T_* \left. \frac{d(S_3/T)}{dT} \right|_{T_*}, \quad (5.1)$$

where  $T_* \approx T_n$  is the finalisation temperature at which the phase transition completes<sup>7</sup>. Typically, for an electroweak phase transition  $\beta/H_* \sim \mathcal{O}(100 - 1000)$ . If  $\beta$  is large, the bubble nucleation rate increases rapidly with the temperature, and the true vacuum then fills the entire space due to bubble nucleation at various different regions. On the other hand, a small  $\beta$  means that the nucleation rate remains approximately constant for the duration of the phase transition, and space is filled by the expansion of the bubbles nucleated at  $T_n$ . In fact, the bubble radius during collision is  $R_* \sim v_w/\beta$ , and since GWs are sourced by the energy in the moving walls and the accompanying fluid motion, a large signal demands small values of  $\beta$ .

Because we are focused on deflagrating bubbles, the main source in our case are the sound waves accompanying bubble expansion and collision [38, 39]. This is because the fluid continues to oscillate and source GWs even after the transition has completed, leading to an amplitude enhancement by a factor  $\mathcal{O}\left(\frac{\beta}{H_*}\right) \sim 100 - 1000$  as compared to the spectrum obtained with the envelope approximation. A thorough analytic treatment of this case is still lacking (see however [99]), but numerical simulations indicate that the amplitude of the spectrum and its peak frequency can be written as [98]<sup>8</sup>

$$h^2 \Omega_{\text{sw}} \simeq 2.65 \times 10^{-6} v_w \left(\frac{H_*}{\beta}\right) \left(\frac{\kappa_v \alpha}{1 + \alpha}\right)^2 \left(\frac{100}{g_*}\right)^{\frac{1}{3}}, \quad (5.2)$$

$$f_{\text{sw}} \simeq 1.9 \times 10^{-2} \text{ mHz} \frac{1}{v_w} \left(\frac{\beta}{H_*}\right) \left(\frac{T}{100 \text{ GeV}}\right) \left(\frac{g_*}{100}\right)^{\frac{1}{6}}. \quad (5.3)$$

Here  $\kappa_v$  is the efficiency in converting the released vacuum energy into bulk motion of the fluid, which can be found in ref. [89] and  $g_* \approx 106.75$  is the number of relativistic degrees of freedom in the plasma.

<sup>7</sup>More precisely, we find that typically  $T_f \approx 0.96 T_n$ , leading to an approximate 75% difference in  $\beta/H$ . However, using the finalisation temperature actually leads to an overestimate of the average bubble radius during collision and consequently of the GW spectrum. We therefore choose to adopt a conservative approach and compute the spectrum at  $T_n$ .

<sup>8</sup>Note that shock waves are expected to develop at a time scale  $\tau_{\text{sh}} \sim \frac{v_w}{\beta} \frac{1}{\sqrt{\kappa_v \alpha}}$  [98, 99], which in our case is not necessarily much larger than the lifetime of the acoustic source,  $\tau_{\text{sw}} \sim H_*^{-1}$  [39], so their effects (including some conversion of acoustic energy into vorticity) would have to be taken into account. However, the dynamics of turbulence generation from sound waves is still poorly understood, and it is difficult to estimate the impact of this effect on the results presented here. We will proceed with the linear sound wave approximation, keeping in mind that more work is needed to fully understand the GW spectrum generated from very strong phase transitions such as the ones considered here.

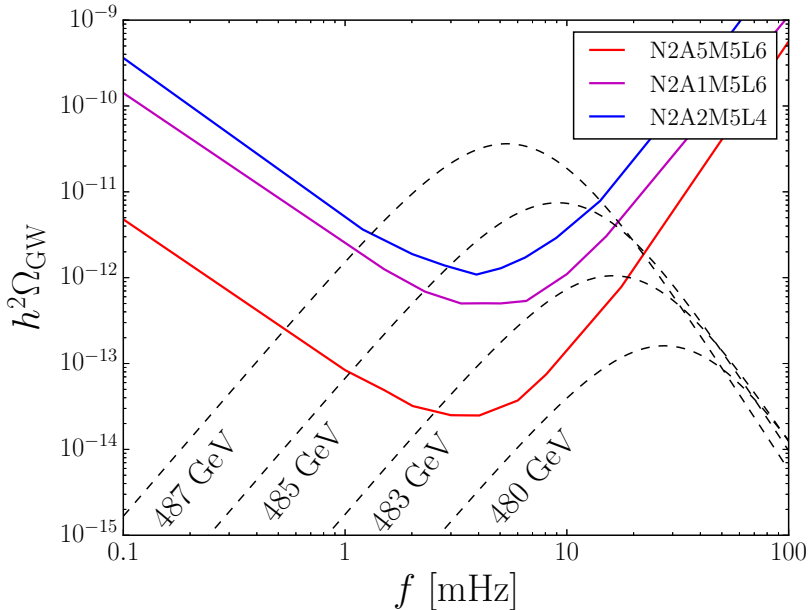


**Figure 3.** Gravitational wave spectrum for differing values of  $m_{A^0} = m_{H^\pm}$ . The solid colored lines are the prospective sensitivity for different LISA configurations (see the text and ref. [98] for more details).

We show in figure 3 the GW spectrum generated by our benchmark scenario with varying values for  $m_{A^0} = m_{H^\pm}$ , with the values of the parameters relevant for obtaining the peak amplitude (5.2) and frequency (5.3) given in Table 1. Figure 3 also shows the prospective sensitivity for different LISA configurations [98, 100]. The LISA Pathfinder mission has successfully established the noise levels expected for the full experiment (N2), and the configuration with three arms (six links, L6) has already been fixed. Thus, the remaining free parameters to be determined are the arm lengths (between 1–5 MKm, A1–A5) and the duration of the mission, which we set at 5 years (M5). For illustrative purposes we also include the sensitivity curve for two arms (four links, L4) with 2 MKm length each (A2). Our results are in the same range as those found *e.g.* in refs. [101, 102] for various other models, provided the phase transition is quite strong, as also in our case.

It is interesting to note that the values for  $\beta/H_*$  obtained in the 2HDM are significantly larger (for comparable values of  $\alpha$ ) than those usually found in other models considered in the GW literature [98, 103]. This is because  $\beta/H_*$  is essentially determined by the temperature dependence of the effective potential, which increases with the number of degrees of freedom present in the plasma, as well as with the strength of their couplings. Indeed, the hierarchical 2HDM considered here involves relatively strong couplings, with the mean field contribution to the thermal potential leading to thermal Higgs masses  $m_T^2/T^2 \sim \frac{\lambda_3}{3} \simeq \frac{2\pi}{3}$ , larger than in weakly coupled scenarios such as supersymmetric extensions.

Finally, we stress that there is some degree of tuning in the results for the GW spectrum, regarding the detectability by LISA. For  $m_{A^0} = 480$  GeV the spectrum is still outside the detectability range of even the most powerful prospective LISA configuration;

for  $m_{A^0} = 487$  GeV the walls are already supersonic and no baryogenesis would be possible; and for  $m_{A^0} \gtrsim 492$  GeV the symmetric vacuum is metastable and no electroweak symmetry breaking takes place.

## 6 Conclusions

We have argued for the possibility that a first order electroweak phase transition could yield the observed baryon asymmetry of the Universe and, at the same time, generate a gravitational wave spectrum observable at LISA. This may be seen as a “proof of principle” for the compatibility of both phenomena, which can coexist for rather strong transitions with relatively slow expanding bubbles, as occurs in 2HDM scenarios. We emphasize that the recent improvements in our understanding of GWs sourced by acoustic waves as well as of the prospective LISA sensitivity were vital for the results presented here. In particular, although the amplitude enhancement by a factor  $\mathcal{O}(\beta/H_*)$  coming from long-lasting sources of GWs has been known for a while [40], a reliable estimate of the dependence of the spectrum with the phase transition parameters and the wall velocity, given in (5.2), could only be achieved with very recent data from extensive numerical simulations [39]. First steps towards an analytic understanding of the problem have been made in [99], but further investigation on the shape of the spectrum is granted, especially for very strong phase transitions.

We have also shown that 2HDMs remain viable candidates for explaining the baryon asymmetry of the Universe, even after the recent stringent bound on the electron EDM by the ACME collaboration. We note however that the experimental constraints on these scenarios are severe, and a significant future increase in the sensitivity of LHC  $A^0 \rightarrow ZH^0$  searches and/or another order-of-magnitude improvement of the eEDM bound will rule out the 2HDM in so far as baryogenesis is concerned.

## Acknowledgments

We like to thank MIAPP for hospitality and an inspiring atmosphere, where this work started, and we thank Germano Nardini and Kimmo Kainulainen for insightful discussions. G.C.D. and T.K. are supported by the German Science Foundation (DFG) under the Collaborative Research Center (SFB) 676 Particles, Strings and the Early Universe. The work of S.H is supported by the Science Technology and Facilities Council (STFC) under grant number ST/L000504/1. J.M.N. is partially supported by the People Programme (Marie Curie Actions) of the European Union Seventh Framework Programme (FP7/2007-2013) under REA grant agreement PIEF-GA-2013-625809, and by the European Research Council under the European Unions Horizon 2020 program, ERC Grant Agreement 648680 (DARKHORIZONS)

**Note added:** While this paper was being prepared for publication, a similar work appeared in the literature claiming the viability of having baryogenesis with a detectable gravitational wave spectrum in the context of a singlet extension [104]. We note that the way friction is

modelled in that work does not seem to lead to a consistent implementation of the runaway phenomenon, thus casting doubt on whether it will lead to a reliable determination of the deflagration/detonation boundary, as is crucial for baryogenesis.

## References

- [1] **WMAP9** , G. Hinshaw et al., “*Nine-year Wilkinson Microwave Anisotropy Probe (WMAP) Observations: Cosmological Parameter Results*,” *The Astrophysical Journal Supplement Series* **208** (Oct., 2013) 19, [[arXiv:1212.5226](#)].
- [2] **Planck** , P. Ade et al., “*Planck 2013 results. XVI. Cosmological parameters*,” *Astron.Astrophys.* **571** (2014) A16, [[arXiv:1303.5076](#)].
- [3] A. Sakharov, “*Violation of CP invariance, C asymmetry, and baryon asymmetry of the Universe*,” *Pisma Zh.Eksp.Teor.Fiz.* **5** (1967) 32–35.
- [4] G. ’t Hooft, “*Symmetry breaking through Bell-Jackiw anomalies*,” *Phys.Rev.Lett.* **37** (1976) 8–11.
- [5] R. Jackiw and C. Rebbi, “*Vacuum periodicity in a Yang-Mills quantum theory*,” *Phys.Rev.Lett.* **37** (1976) 172–175.
- [6] F. R. Klinkhamer and N. Manton, “*A Saddle Point Solution in the Weinberg-Salam Theory*,” *Phys.Rev.* **D30** (1984) 2212.
- [7] S. Weinberg, “*Gauge and global symmetries at high temperature*,” *Phys.Rev.* **D9** (1974) 3357–3378.
- [8] L. Dolan and R. Jackiw, “*Symmetry behavior at finite temperature*,” *Phys.Rev.* **D9** (1974) 3320–3341.
- [9] G. W. Anderson and L. J. Hall, “*The electroweak phase transition and baryogenesis*,” *Phys.Rev.* **D45** (1992) 2685–2698.
- [10] V. Kuzmin, V. Rubakov, and M. Shaposhnikov, “*On the Anomalous Electroweak Baryon Number Nonconservation in the Early Universe*,” *Phys. Lett.* **B155** (1985) 36.
- [11] T. Konstandin, “*Quantum Transport and Electroweak Baryogenesis*,” *Phys. Usp.* **56** (2013) 747 [*Usp. Fiz. Nauk* **183** (2013) 785] [[arXiv:1302.6713](#) [[hep-ph](#)]].
- [12] K. Kajantie, M. Laine, K. Rummukainen, and M. E. Shaposhnikov, “*Is there a hot electroweak phase transition at  $m(H)$  larger or equal to  $m(W)$ ?*,” *Phys.Rev.Lett.* **77** (1996) 2887–2890, [[hep-ph/9605288](#)].
- [13] M. D’Onofrio, K. Rummukainen, and A. Tranberg, “*The Sphaleron Rate in the Minimal Standard Model*,” *Phys.Rev.Lett.* **113** (2014) 141602, [[arXiv:1404.3565](#)].
- [14] C. Jarlskog, “*Commutator of the Quark Mass Matrices in the Standard Electroweak Model and a Measure of Maximal CP Violation*,” *Phys.Rev.Lett.* **55** (1985) 1039.
- [15] **Particle Data Group** , K. Olive et al., “*Review of Particle Physics*,” *Chin.Phys.* **C38** (2014) 090001.
- [16] M. Gavela, P. Hernandez, J. Orloff, and O. Pene, “*Standard model CP violation and baryon asymmetry*,” *Mod.Phys.Lett.* **A9** (1994) 795–810, [[hep-ph/9312215](#)].

- [17] M. Gavela, P. Hernandez, J. Orloff, O. Pene, and C. Quimbay, “Standard model CP violation and baryon asymmetry. Part 2: Finite temperature,” *Nucl.Phys.* **B430** (1994) 382–426, [[hep-ph/9406289](#)].
- [18] P. Huet and E. Sather, “Electroweak baryogenesis and standard model CP violation,” *Phys.Rev.* **D51** (1995) 379–394, [[hep-ph/9404302](#)].
- [19] **ACME**, J. Baron et al., “Order of Magnitude Smaller Limit on the Electric Dipole Moment of the Electron,” *Science* **343** (2014) 269–272, [[arXiv:1310.7534](#)].
- [20] T. Alanne, K. Kainulainen, K. Tuominen, and V. Vaskonen, “Baryogenesis in the two doublet and inert singlet extension of the Standard Model,” *JCAP* **1608** (2016), no. 08 057, [[arXiv:1607.03303](#)].
- [21] L. D. McLerran, M. E. Shaposhnikov, N. Turok, and M. B. Voloshin, “Why the baryon asymmetry of the universe is approximately  $10^{-10}$ ,” *Phys. Lett.* **B256** (1991) 451–456.
- [22] N. Turok and J. Zadrozny, “Electroweak baryogenesis in the two doublet model,” *Nucl.Phys.* **B358** (1991) 471–493.
- [23] A. G. Cohen, D. Kaplan, and A. Nelson, “Spontaneous baryogenesis at the weak phase transition,” *Phys. Lett.* **B263** (1991) 86–92.
- [24] J. M. Cline and P.-A. Lemieux, “Electroweak phase transition in two Higgs doublet models,” *Phys.Rev.* **D55** (1997) 3873–3881, [[hep-ph/9609240](#)].
- [25] L. Fromme, S. J. Huber, and M. Seniuch, “Baryogenesis in the two-Higgs doublet model,” *JHEP* **0611** (2006) 038, [[hep-ph/0605242](#)].
- [26] J. M. Cline, K. Kainulainen, and M. Trott, “Electroweak baryogenesis in two Higgs doublet models and B meson anomalies,” *JHEP* **1111** (2011) 089, [[arXiv:1107.3559](#)].
- [27] J. Shu and Y. Zhang, “Impact of a CP Violating Higgs Sector: From LHC to Baryogenesis,” *Phys.Rev.Lett.* **111** (2013), no. 9 091801, [[arXiv:1304.0773](#)].
- [28] G. C. Dorsch, S. J. Huber, and J. M. No, “A strong electroweak phase transition in the 2HDM after LHC8,” *JHEP* **1310** (2013) 029, [[arXiv:1305.6610](#)].
- [29] G. Dorsch, S. Huber, K. Mimasu, and J. No, “Echoes of the Electroweak Phase Transition: Discovering a second Higgs doublet through  $A_0 \rightarrow ZH_0$ ,” *Phys.Rev.Lett.* **113** (2014), no. 21 211802, [[arXiv:1405.5537](#)].
- [30] G. C. Dorsch, S. J. Huber, K. Mimasu, and J. M. No, “Hierarchical vs Degenerate 2HDM: The LHC Run 1 Legacy at the Onset of Run 2,” *Phys. Rev.* **D93** (2016), no. 11 115033, [[arXiv:1601.04545](#)].
- [31] M. Jung and A. Pich, “Electric Dipole Moments in Two-Higgs-Doublet Models,” *JHEP* **1404** (2014) 076, [[arXiv:1308.6283](#)].
- [32] S. Ipek, “Perturbative analysis of the electron electric dipole moment and CP violation in two-Higgs-doublet models,” *Phys. Rev.* **D89** (2014), no. 7 073012, [[arXiv:1310.6790](#)].
- [33] S. Inoue, M. J. Ramsey-Musolf, and Y. Zhang, “CP-violating phenomenology of flavor conserving two Higgs doublet models,” *Phys. Rev.* **D89** (2014), no. 11 115023, [[arXiv:1403.4257](#)].
- [34] M. Kamionkowski, A. Kosowsky, and M. S. Turner, “Gravitational radiation from first order phase transitions,” *Phys.Rev.* **D49** (1994) 2837–2851, [[astro-ph/9310044](#)].



- [35] P. Amaro-Seoane et al., “*eLISA/NGO: Astrophysics and cosmology in the gravitational-wave millihertz regime*,” *GW Notes* **6** (2013) 4–110, [[arXiv:1201.3621](#)].
- [36] **Virgo, LIGO Scientific**, B. P. Abbott et al., “*Observation of Gravitational Waves from a Binary Black Hole Merger*,” *Phys. Rev. Lett.* **116** (2016), no. 6 061102, [[arXiv:1602.03837](#)].
- [37] **Virgo, LIGO Scientific**, B. P. Abbott et al., “*GW151226: Observation of Gravitational Waves from a 22-Solar-Mass Binary Black Hole Coalescence*,” *Phys. Rev. Lett.* **116** (2016), no. 24 241103, [[arXiv:1606.04855](#)].
- [38] M. Hindmarsh, S. J. Huber, K. Rummukainen, and D. J. Weir, “*Gravitational waves from the sound of a first order phase transition*,” *Phys. Rev. Lett.* **112** (2014) 041301, [[arXiv:1304.2433](#)].
- [39] M. Hindmarsh, S. J. Huber, K. Rummukainen, and D. J. Weir, “*Numerical simulations of acoustically generated gravitational waves at a first order phase transition*,” *Phys. Rev.* **D92** (2015), no. 12 123009, [[arXiv:1504.03291](#)].
- [40] C. Caprini, R. Durrer, and G. Servant, “*The stochastic gravitational wave background from turbulence and magnetic fields generated by a first-order phase transition*,” *JCAP* **0912** (2009) 024, [[arXiv:0909.0622](#)].
- [41] E. Thrane and J. D. Romano, “*Sensitivity curves for searches for gravitational-wave backgrounds*,” *Phys. Rev.* **D88** (2013), no. 12 124032, [[arXiv:1310.5300](#)].
- [42] S. L. Glashow and S. Weinberg, “*Natural conservation laws for neutral currents*,” *Phys.Rev.* **D15** (1977) 1958.
- [43] T. Cheng and M. Sher, “*Mass Matrix Ansatz and Flavor Nonconservation in Models with Multiple Higgs Doublets*,” *Phys.Rev.* **D35** (1987) 3484.
- [44] A. Pich and P. Tuzon, “*Yukawa alignment in the two-Higgs-doublet model*,” *Phys.Rev.* **D80** (2009) 091702, [[arXiv:0908.1554](#)].
- [45] G. Branco, W. Grimus, and L. Lavoura, “*Relating the scalar flavor changing neutral couplings to the CKM matrix*,” *Phys. Lett.* **B380** (1996) 119–126, [[hep-ph/9601383](#)].
- [46] G. D’Ambrosio, G. Giudice, G. Isidori, and A. Strumia, “*Minimal flavor violation: an effective field theory approach*,” *Nucl.Phys.* **B645** (2002) 155–187, [[hep-ph/0207036](#)].
- [47] F. Botella, G. Branco, and M. Rebelo, “*Minimal flavour violation and multi-Higgs models*,” *Phys. Lett.* **B687** (2010) 194–200, [[arXiv:0911.1753](#)].
- [48] A. J. Buras, M. V. Carlucci, S. Gori, and G. Isidori, “*Higgs-mediated FCNCs: Natural Flavour Conservation vs. Minimal Flavour Violation*,” *JHEP* **1010** (2010) 009, [[arXiv:1005.5310](#)].
- [49] L. J. Hall and M. B. Wise, “*Flavor changing Higgs-boson couplings*,” *Nucl. Phys.* **B187** (1981) 397–408.
- [50] G. Branco, P. Ferreira, L. Lavoura, M. Rebelo, M. Sher, et al., “*Theory and phenomenology of two-Higgs-doublet models*,” *Phys.Rept.* **516** (Dec., 2012) 1–102, [[arXiv:1106.0034](#)].
- [51] J. Diaz-Cruz and A. Mendez, “*Vacuum alignment in multiscalar models*,” *Nucl.Phys.* **B380** (1992) 39–50.
- [52] S. Davidson and H. E. Haber, “*Basis-independent methods for the two-Higgs-doublet model*,” *Phys.Rev.* **D72** (2005) 035004; Erratum–*ibid.* **D72** (2005) 099902, [[hep-ph/0504050](#)].

- [53] L. Lavoura and J. P. Silva, “Fundamental CP violating quantities in a  $SU(2) \times U(1)$  model with many Higgs doublets,” *Phys. Rev.* **D50** (1994) 4619–4624, [[hep-ph/9404276](#)].
- [54] **ATLAS Collaboration**, G. Aad et al., “Observation of a new particle in the search for the Standard Model Higgs boson with the ATLAS detector at the LHC,” *Phys. Lett.* **B716** (2012) 1–29, [[arXiv:1207.7214](#)].
- [55] **CMS Collaboration**, S. Chatrchyan et al., “Observation of a new boson at a mass of 125 GeV with the CMS experiment at the LHC,” *Phys. Lett.* **B716** (2012) 30–61, [[arXiv:1207.7235](#)].
- [56] J. F. Gunion and H. E. Haber, “The CP conserving two Higgs doublet model: The Approach to the decoupling limit,” *Phys.Rev.* **D67** (2003) 075019, [[hep-ph/0207010](#)].
- [57] W. Grimus, L. Lavoura, O. Ogreid, and P. Osland, “A Precision constraint on multi-Higgs-doublet models,” *J.Phys.* **G35** (2008) 075001, [[arXiv:0711.4022](#)].
- [58] W. Grimus, L. Lavoura, O. Ogreid, and P. Osland, “The Oblique parameters in multi-Higgs-doublet models,” *Nucl.Phys.* **B801** (2008) 81–96, [[arXiv:0802.4353](#)].
- [59] M. Gorbahn, J. M. No and V. Sanz, “Benchmarks for Higgs Effective Theory: Extended Higgs Sectors,” *JHEP* **10** (2015) 036, [[arXiv:1502.07352](#)].
- [60] H. E. Haber and D. O’Neil, “Basis-independent methods for the two-Higgs-doublet model III: The CP-conserving limit, custodial symmetry, and the oblique parameters  $S$ ,  $T$ ,  $U$ ,” *Phys.Rev.* **D83** (2011) 055017, [[arXiv:1011.6188](#)].
- [61] G. Funk, D. O’Neil, and R. M. Winters, “What the oblique parameters  $S$ ,  $T$ , and  $U$  and their extensions reveal about the 2HDM: A numerical analysis,” *Int.J.Mod.Phys.* **A27** (2012) 1250021, [[arXiv:1110.3812](#)].
- [62] F. Mahmoudi and O. Stal, “Flavor constraints on the two-Higgs-doublet model with general Yukawa couplings,” *Phys.Rev.* **D81** (2010) 035016, [[arXiv:0907.1791](#)].
- [63] T. Enomoto and R. Watanabe, “Flavor constraints on the Two Higgs Doublet Models of  $Z_2$  symmetric and aligned types,” *JHEP* **05** (2016) 002, [[arXiv:1511.05066](#)].
- [64] T. Hermann, M. Misiak, and M. Steinhauser, “ $\bar{B} \rightarrow X_s \gamma$  in the Two Higgs Doublet Model up to Next-to-Next-to-Leading Order in QCD,” *JHEP* **1211** (2012) 036, [[arXiv:1208.2788](#)].
- [65] M. Misiak et al., “Updated NNLO QCD predictions for the weak radiative B-meson decays,” *Phys. Rev. Lett.* **114** (2015), no. 22 221801, [[arXiv:1503.01789](#)].
- [66] J. Engel, M. J. Ramsey-Musolf, and U. van Kolck, “Electric Dipole Moments of Nucleons, Nuclei, and Atoms: The Standard Model and Beyond,” *Prog.Part.Nucl.Phys.* **71** (2013) 21–74, [[arXiv:1303.2371](#)].
- [67] S. Weinberg, “Larger Higgs Exchange Terms in the Neutron Electric Dipole Moment,” *Phys. Rev. Lett.* **63** (1989) 2333.
- [68] T. Abe, J. Hisano, T. Kitahara, and K. Tobioka, “Gauge invariant Barr-Zee type contributions to fermionic EDMs in the two-Higgs doublet models,” [arXiv:1311.4704](#).
- [69] W. Dekens and J. de Vries, “Renormalization Group Running of Dimension-Six Sources of Parity and Time-Reversal Violation,” *JHEP* **1305** (2013) 149, [[arXiv:1303.3156](#)].
- [70] K. Chetyrkin, B. A. Kniehl, and M. Steinhauser, “Decoupling relations to  $\mathcal{O}(\alpha_s^3)$  and their connection to low-energy theorems,” *Nucl.Phys.* **B510** (1998) 61–87, [[hep-ph/9708255](#)].

- [71] J. J. Hudson, D. M. Kara, I. J. Smallman, B. E. Sauer, M. R. Tarbutt, and E. A. Hinds, “Improved measurement of the shape of the electron,” *Nature* **473** (2011) 493–496.
- [72] C. Baker, D. Doyle, P. Geltenbort, K. Green, M. van der Grinten, et al., “An Improved experimental limit on the electric dipole moment of the neutron,” *Phys.Rev.Lett.* **97** (2006) 131801, [[hep-ex/0602020](#)].
- [73] K. Klimenko, “On Necessary and Sufficient Conditions for Some Higgs Potentials to Be Bounded From Below,” *Theor.Math.Phys.* **62** (1985) 58–65.
- [74] M. Maniatis, A. von Manteuffel, O. Nachtmann, and F. Nagel, “Stability and symmetry breaking in the general two-Higgs-doublet model,” *Eur.Phys.J.* **C48** (2006) 805–823, [[hep-ph/0605184](#)].
- [75] G. C. Dorsch, S. J. Huber, K. Mimasu, J. M. No, *To Appear*.
- [76] A. Arhrib, “Unitarity constraints on scalar parameters of the standard and two Higgs doublets model,” [hep-ph/0012353](#).
- [77] I. Ginzburg and I. Ivanov, “Tree level unitarity constraints in the 2HDM with CP violation,” [hep-ph/0312374](#).
- [78] I. Ginzburg and I. Ivanov, “Tree-level unitarity constraints in the most general 2HDM,” *Phys.Rev.* **D72** (2005) 115010, [[hep-ph/0508020](#)].
- [79] V. Khachatryan *et al.* [CMS Collaboration], “Search for neutral resonances decaying into a Z boson and a pair of b jets or tau leptons,” *Phys. Lett.* **B759** (2016) 369, [[arXiv:1603.02991](#)].
- [80] A. D. Linde, “Fate of the false vacuum at finite temperature: theory and applications,” *Phys. Lett.* **B100** (1981) 37.
- [81] A. Kusenko, “Improved action method for analyzing tunneling in quantum field theory,” *Phys. Lett.* **B358** (1995) 51–55, [[hep-ph/9504418](#)].
- [82] P. John, “Bubble wall profiles with more than one scalar field: A Numerical approach,” *Phys. Lett.* **B452** (1999) 221–226, [[hep-ph/9810499](#)].
- [83] J. M. Cline, G. D. Moore, and G. Servant, “Was the electroweak phase transition preceded by a color broken phase?,” *Phys. Rev.* **D60** (1999) 105035, [[hep-ph/9902220](#)].
- [84] T. Konstandin and S. J. Huber, “Numerical approach to multi dimensional phase transitions,” *JCAP* **0606** (2006) 021, [[hep-ph/0603081](#)].
- [85] L. Fromme and S. J. Huber, “Top transport in electroweak baryogenesis,” *JHEP* **0703** (2007) 049, [[hep-ph/0604159](#)].
- [86] S. J. Huber, P. John, M. Laine, and M. G. Schmidt, “CP violating bubble wall profiles,” *Phys. Lett.* **B475** (2000) 104–110, [[hep-ph/9912278](#)].
- [87] S. J. Huber and M. Sopena, “The bubble wall velocity in the minimal supersymmetric light stop scenario,” *Phys. Rev.* **D85** (2012) 103507, [[arXiv:1112.1888](#)].
- [88] D. Bodeker and G. D. Moore, “Can electroweak bubble walls run away?,” *JCAP* **0905** (2009) 009, [[arXiv:0903.4099](#)].
- [89] J. R. Espinosa, T. Konstandin, J. M. No, and G. Servant, “Energy Budget of Cosmological First-order Phase Transitions,” *JCAP* **1006** (2010) 028, [[arXiv:1004.4187](#)].

- [90] D. Bodeker, L. Fromme, S. J. Huber, and M. Seniuch, “*The Baryon asymmetry in the standard model with a low cut-off*,” *JHEP* **02** (2005) 026, [[hep-ph/0412366](#)].
- [91] J. R. Espinosa, B. Gripaios, T. Konstandin and F. Riva, “*Electroweak Baryogenesis in Non-minimal Composite Higgs Models*,” *JCAP* **1201** (2012) 012 [[arXiv:1110.2876](#) [[hep-ph](#)]].
- [92] T. Prokopec, M. G. Schmidt, and S. Weinstock, “*Transport equations for chiral fermions to order  $\hbar$  and electroweak baryogenesis. Part 1*,” *Annals Phys.* **314** (2004) 208–265, [[hep-ph/0312110](#)].
- [93] T. Konstandin, G. Nardini, and I. Rues, “*From Boltzmann equations to steady wall velocities*,” *JCAP* **1409** (2014), no. 09 028, [[arXiv:1407.3132](#)].
- [94] J. M. Cline, M. Joyce, and K. Kainulainen, “*Supersymmetric electroweak baryogenesis in the WKB approximation*,” *Phys. Lett.* **B417** (1998) 79–86, [[hep-ph/9708393](#)]. [Erratum: *Phys. Lett.* **B448**,321(1999)].
- [95] J. M. Cline, M. Joyce, and K. Kainulainen, “*Supersymmetric electroweak baryogenesis*,” *JHEP* **07** (2000) 018, [[hep-ph/0006119](#)].
- [96] K. Kainulainen, T. Prokopec, M. G. Schmidt, and S. Weinstock, “*First principle derivation of semiclassical force for electroweak baryogenesis*,” *JHEP* **06** (2001) 031, [[hep-ph/0105295](#)].
- [97] J. M. No, “*Large Gravitational Wave Background Signals in Electroweak Baryogenesis Scenarios*,” *Phys. Rev.* **D84** (2011) 124025, [[arXiv:1103.2159](#)].
- [98] C. Caprini et al., “*Science with the space-based interferometer eLISA. II: Gravitational waves from cosmological phase transitions*,” *JCAP* **1604** (2016), no. 04 001, [[arXiv:1512.06239](#)].
- [99] M. Hindmarsh, “*Sound shell model for acoustic gravitational wave production at a first-order phase transition in the early Universe*,” [arXiv:1608.04735](#).
- [100] A. Klein et al., “*Science with the space-based interferometer eLISA: Supermassive black hole binaries*,” *Phys. Rev.* **D93** (2016), no. 2 024003, [[arXiv:1511.05581](#)].
- [101] K. Hashino, M. Kakizaki, S. Kanemura and T. Matsui, *Phys. Rev. D* **94** (2016) no.1, 015005 [[arXiv:1604.02069](#) [[hep-ph](#)]].
- [102] P. Huang, A. J. Long, and L.-T. Wang, “*Probing the Electroweak Phase Transition with Higgs Factories and Gravitational Waves*,” [arXiv:1608.06619](#).
- [103] S. J. Huber and T. Konstandin, “*Production of gravitational waves in the nMSSM*,” *JCAP* **0805** (2008) 017, [[arXiv:0709.2091](#)].
- [104] V. Vaskonen, “*Electroweak baryogenesis and gravitational waves from a real scalar singlet*,” [arXiv:1611.02073](#).